PCCP

Molecular dynamics study of pressure-driven water transport through graphene bilayers

Journal:	*Physical Chemistry Chemical Physics*
Manuscript ID	CP-ART-08-2015-004976.R1
Article Type:	Paper
Date Submitted by the Author:	28-Oct-2015

Complete List of Authors:	Liu, Bo; Nanyang Technological University, Wu, Renbing; Nanyang Technological University, DHI-NTU Center, Nanyang Environment and Water Research Institute Baimova, Julia; Nanyang Technological University, Wu, Hong; Central South University, State Key Laboratory of Powder Metallurgy Law, Wing; Nanyang Technological University, School of Civil and Environmental Engineering Dmitriev, Sergey; Institute for Metals Superplasticity Problems, Zhou, Kun; Nanyang Technological University, School of Mechanical and Aerospace Engineering

Molecular dynamics study of pressure-driven water transport through graphene bilayers

Bo Liu,[a,b] Renbing Wu,[a,b] Julia A. Baimova,[c] Hong Wu,[d] Adrian Wing-Keung Law, *[a,e] Sergey V. Dmitriev,[c, f] Kun Zhou*[a,b]

[a] *DHI-NTU Center, Nanyang Environment and Water Research Institute, Nanyang Technological University, 50 Nanyang Avenue, Singapore 639798, Singapore*

[b] *School of Mechanical and Aerospace Engineering, Nanyang Technological University, 50 Nanyang Avenue, Singapore 639798, Singapore*

[c] *Institute for Metals Superplasticity Problems, Russian Academy of Sciences, Ufa 450001, Russia*

[d] *State Key Laboratory of Powder Metallurgy, Central South University, Changsha, Hunan 410083, People's Republic of China*

[e] *School of Civil and Environmental Engineering, Nanyang Technological University, 50 Nanyang Avenue, Singapore 639798, Singapore*

[f] *St.Petersburg State Polytechnical UniversityI*, *Polytechnicheskaya* 29, *St. Petersburg* 195251, *Russia*

Abstract

The pressure-driven water transport inside the nanochannel formed by GE bilayers is studied via molecular dynamics simulation. The effects of flow driving pressure, channel size, as well as interaction strength between the water molecules and the GE bilayer are investigated and understood by exploring the distribution of the water molecules, their average velocity, and the friction between them and the channel walls. Ultrafast water flow rate is observed and different channel-size dependences of the water flow rate are discovered for weak and strong interaction strengths. The layered water structure inside the GE bilayer is found to play significant role in affecting the water flow rate. This study is of significance for the design and application of GE-based nanomaterials in future nanofiltration and water purification technologies.

* Corresponding authors: Adrian Wing-Keung Law, Tel./Fax: +65 6790 5296;
Email address: cwklaw@ntu.edu.sg
Kun Zhou, Tel.: +65 6790 5499; Fax: +65 6792 4062
Email address: kzhou@ntu.edu.sg

1. Introduction

In the broad field of nanotechnology, nanofluidics has attracted intensive attention recent years due to many of its promising applications such as water desalination and purification,[1, 2] biosensing,[3, 4] nanoprinting [5] and nanolithography.[6] The basis of most of these applications relies on the unique properties of nanoconfined fluids which are not achievable in the microscopic or macroscopic fluids. When fluids are confined in nanopores or nanochannels with sizes ranging from sub-nanometer to several nanometers, the interactions among the fluid ions or molecules change dramatically due to their close contact with the confining walls and their unique spatial distribution at the nanoscale. The change of such interactions would result in unconventional and sometimes even counterintuitive behaviors of the fluids.[7]

One good example would be the water streams inside carbon nanotubes (CNT). Previous studies have demonstrated that the transport viscosity of water confined in CNT is orders of magnitude lower than that of the bulk water,[8] leading to the ultrafast water flow rate in CNT which is comparable to that in biological channels such as aquaporins.[9, 10] The hydrogen bonding among the water molecules and the inherent smoothness of the interior wall of the CNT were identified as the crucial reasons for the low viscosity and ultrafast flow rate.[11, 12] Moreover, by changing the diameter of the CNT, the transport behavior of fluids inside it becomes tunable due to the adjustment of the CNT wall curvature.[13]

Although the previous studies on nanoconfined nanofluid have explored many interesting phenomena, most of these studies were focused on one-dimensional nano-systems such as nanopores and nanotubes. Only a few works have been reported on fluids transport behaviors in two-dimensional nanochannels. Recently, graphene (GE) derived functional membranes obtained by stacking functionalized GE nanosheets have been identified to be excellent candidate

materials for nanofiltration and separation applications because of their ultimate thinness, high flexibility, strong mechanical strength and tunable porous structures.[14-18] In its dry state, the GE oxide (GO) membrane made by vacuum filtration can be so tightly stacked that an average interlayer distance less than ~0.7 nm can be obtained. For such narrow interlayer distance, only water molecules aligned in a monolayer pattern can permeate through the nanochannels between the neighboring GO nanosheets, while hydrated ions with larger radii than the water molecule are blocked.[15] By adjusting the interlayer distance between the GO nanosheets through interlayer intercalation, a broad spectrum of GO membranes could be produced to precisely separate the target ions and molecules with specific sizes from the bulk solution.[16, 19]

Interestingly, though being severely confined in the narrow interlayer space, water molecules permeate through this nanoconfined space with unexpectedly high permeability.[15] This high water permeability makes GO membranes more promising to be used as an ideal material for water desalination and purification. By intercalating nanoparticles such as CNT into the interlayer space between the GO nanosheets, it was reported that a high water flux of around 11 L m^{-2} h^{-1} bar^{-1} can be obtained while keeping nearly 100% rejection of dye molecules and upto 85% rejection of salt ions.[19] The individual GO nanosheets have two types of domains: functionalized (oxidized) GE and pristine GE. It is believed that the high water permeability of the GO membranes is attributed to the capillary network formed by the pristine domains which allow nearly frictionless flow of a layer of water.[14] Later, Wei *et al.* conducted molecular dynamics (MD) simulations and demonstrated that the fast water transport through the pristine domains can be significantly affected by a prominent pinning effect at the interface between the functionalized and pristine domains in the GO nanosheets.[20] Moreover, it was also proposed that the structural parameters, including interlayer distance, nanochannel length and pore

concentration may play a significant role in determining the water permeability through the GO membranes.[20]

To further understand the permeation characteristics through the GO membranes, especially through the capillary network formed by the pristine GE domains, this study investigates the water transport behaviors through the nanochannels in GE bilayers using MD simulations. Several structural parameters of the bilayer including the interlayer distance and nanochannel length, are considered. In addition, the effects of pressure and water/GE interaction strength are also investigated. The result from the present study would not only provide guidance for novel engineering membrane design, but also contribute to promote the application of GO membranes in future water desalination and purification technologies.

2. Simulation modeling

The configuration of the simulation system consists of three parts: two water reservoirs at the two ends and the nanochannel formed by the GE bilayer and four constraint walls in the middle, as shown in Fig.1. Both water reservoirs have the same dimension of 40×37×38 $Å^3$ and 1880 water molecules are placed in each water reservoirs to produce a mass density of 1 g/cm^3. The GE bilayer which connects the two water reservoirs is set to be parallel to the *x*y plane and has its center at z = 19 Å. The lattice constant of GE bilayer is set to be 1.42 Å. The interlayer space of the GE bilayer provides the nanochannel for water transport. The nanochannel thickness, i.e., the interlayer distance of the bilayer, is denoted as d, while the nanochannel length is denoted as L. Two GE nanosheets are placed at each end of the GE bilayer and set to be normal to the bilayer plane to serve as the constraint walls which restrict the water molecules movement.

All the simulations are conducted by using the large-scale atomic/molecular massively parallel simulator (LAMMPS) package.[21] Periodic boundary conditions are applied in all three directions. The Transferable Intermolecular Potential 3P (TIP3P) water model[22] is adopted to construct the water molecules with the partial charges of the O and H atoms set to be -0.834e and 0.417e, respectively. The CHARMM27 force field[23] is used to describe both the bonded and non-bonded interatomic interactions between the O and H atoms. The total energy of a system described by the CHARMM27 force field can be expresses as[23]

$$E_{total} = E_{bonds} + E_{angles} + E_{dihedrals} + E_{impropers} + E_{Urey-Bradley} + E_{vdW} + E_{elec} \quad . \qquad (1)$$

The first five terms account for the intramolecular interactions (bond stretch, bond angle, dihedral angle, improper angle and Urey-Bradley) that characterize the short-range bonding. The last two terms are associated with the long-range intermolecular interactions, including the electrostatic and the van der Waals (vdW) interactions.

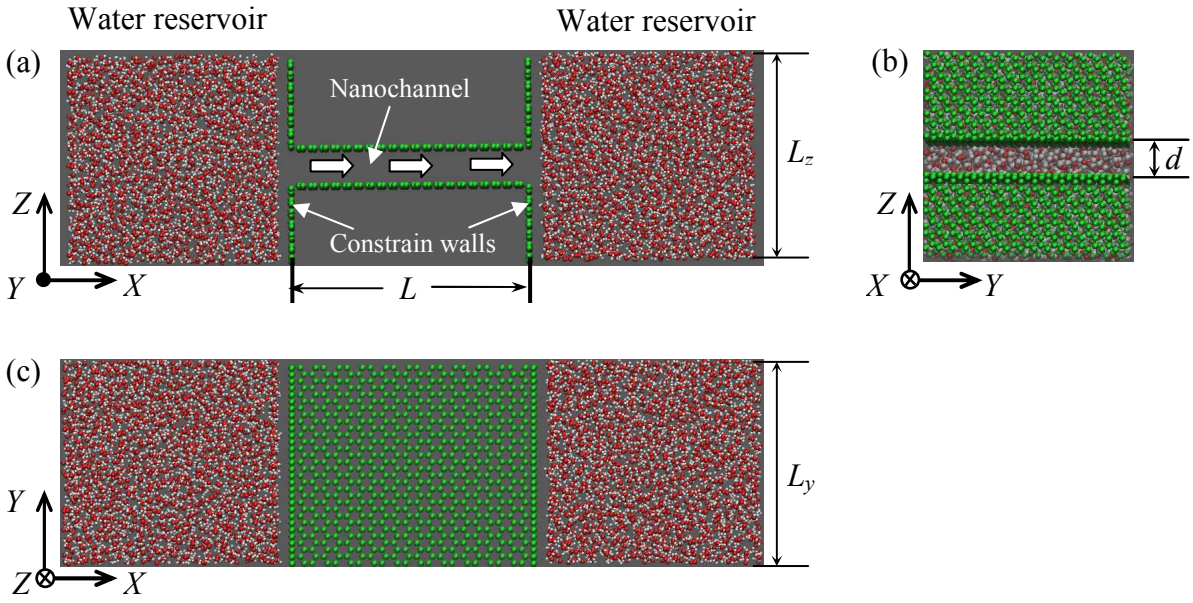

Fig.1. (a) Front, (b) side and (c) top views of the simulation configuration. Two water reservoirs are connected by the GE bilayer that parallel to the *xy* plane and four constrain walls are set to be normal to the GE bilayer to restrict the water molecules movement. The green, red and white colors represent the C, O and H atoms, respectively.

The long-range electrostatic interactions are computed with the particle-particle particle-mesh (PPPM) method with a cutoff distance of 12 Å and a root mean square accuracy of 10^{-4}. The interaction between the GE bilayer and water molecules is modeled as vdW interactions between the C and O atoms, while the interaction among the water molecules is modeled as vdW interactions of the H-O, H-H and O-O atom pairs. In this study, all the vdW interactions are described by the 12-6 Lennard-Jones potential as

$$V(r) = 4\chi\varepsilon\left[\left(\frac{\sigma}{r}\right)^{12} - \left(\frac{\sigma}{r}\right)^{6}\right] \quad . \tag{2}$$

Here, r represents the distance of two atoms, ε is the energy well that reflects their interaction strength, σ denotes the zero-across distance of the potential, and χ is a scaling factor and can be used to tune the interface interaction strength. For the pair interactions of O-O, O-H and H-H, χ is kept as 1, which means that these interactions are maintained as original. For the pair interactions of C-O, χ is changed in the range of 1 to 4 to study the effect of GE/water interaction strength on the water transport behaviors. The values of σ and ε for the pair interactions of H-O, H-H and O-O are adopted as $\varepsilon_{\mathrm{O-O}} = 0.1521$ kcal/mol, $\sigma_{\mathrm{O-O}} = 3.15$ Å, $\varepsilon_{\mathrm{O-H}} = 0.0836$ Kcal/mol, $\sigma_{\mathrm{O-H}} = 1.77$ Å, $\varepsilon_{\mathrm{H-H}} = 0.0461$ Kcal/mol and $\sigma_{\mathrm{H-H}} = 0.40$ Å, according to the CHARMM27 force field [23], while the values of σ and ε for the C-O interaction are adopted as $\varepsilon_{\mathrm{C-O}} = 0.0937$ Kcal/mol and $\sigma_{\mathrm{C-O}} = 3.19$ Å. By using this C-O interaction parameter set, it has been reported that the experimentally observed contact angle of water droplet on a GE nanosheet can be well reproduced.[24] The cutoff distance for the vdW interactions is set as 10 Å which is about 3 times of $\sigma_{\mathrm{C-O}} = 3.19$ Å.

All the simulations are performed under the constant volume and temperature (NVT) ensemble with the temperature kept at 300 K using the Nosé-hoover thermostat. The temperature is calculated with the center-of-mass velocity subtracted. In order to reveal the intrinsic transport behaviors of the water molecules through the GE bilayer, its flexibility is not considered during the simulation by treating the bilayer as a rigid body with the positions of the C atoms fixed. Initially, the water molecules are relaxed for 50 ps with a timestep of 0.5 fs to reach an equilibrium state. Afterwards, a driving pressure is imposed on the system to generate a flow through the nanochannel by applying a force f along the positive X-direction on all the O atoms in the left water reservoir. For a desired pressure difference ΔP between the two ends of the nanochannel, the force f is calculated as[25]

$$f = \Delta P L_y L_z / n \quad . \tag{3}$$

Here, n is the number of the O atoms in the left water reservoir, $L_y L_z$ accounts for its cross section area as shown in Fig. 1. This method has been used in many previous studies to simulate the transport behaviors of nanoconfined water flow.[20, 26-28] Pressure differences of 5-7 MPa are generally used in practical industrial filtration process, but the resulting flow rates are too slow for MD to accurately resolve over a practical timescale. Therefore, in this study, the pressure difference ΔP in the range of 100 to 500 MPa is applied. Such a large pressure difference is required to resolve the dynamics of the water molecules over a relatively short time period due to the large computational cost associated with MD simulation. With the force f imposed, the simulation is conducted for 250 ps to obtain a steady water flow. Upon reaching the steady state, the simulation is conducted for another 250 ps for data collection. It is found that the simulation duration of 250 ps after the steady state is large enough to obtain well-converged and accurate simulation results.

3. Results and discussion

3.1. Fast water transport in GE bilayer

At the steady state, the number N of water molecules in the nanochannel and their average velocity $\bar{v}$ along the X-direction remain constant with slight fluctuations. The flow rate Q is defined as the number of water molecules that transmit through the right end of the nanochannel per unit time per unit area. In this study, Q can be estimated as

$$Q = \frac{\bar{v}N}{dL_y L} \quad . \tag{4}$$

Figure 2 shows the dependence of Q on the applied pressure difference ΔP for the case of $L = 51$ Å and $d = 10$ Å. It is observed that Q increases linearly with ΔP, which gives the possibility to obtain the water flow rate at low ΔP through linear extrapolation.

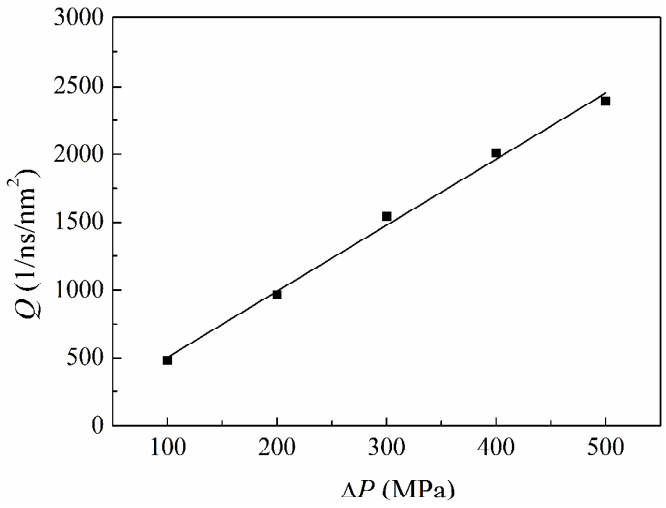

Fig. 2. Dependence of flow rate Q on pressure difference ΔP.

For $\Delta P = 5$MPa which is typically used for industrial nanofiltration membranes, Q is obtained as 41.89 $(nm^2ns)^{-1}$ through the linear extrapolation. This value is more than 20 times

larger than that obtained for the (12,12) CNT under the same pressure as reported by a recent MD study.[29] At large $\Delta P = 200$ MPa , Q is obtained as 990 $(nm^2ns)^{-1}$ which is also much larger than those in the range of ~410-700 $(nm^2ns)^{-1}$ reported for the CNT with its diameter in the range of 1.35-2.17 nm.[30] These results indicate that layered GE nanosheets may be superior over nanotubes for nanoscale water transmission.

Previous studies have demonstrated that the water flow in CNT is significantly enhanced and exhibits much larger flow rate than that predicted by the Hagen-Poiseuille (HP) equation of continuum mechanics. Such enhancement has been attributed to the modification of the assumption of nonslip boundary condition as well as to the dramatic change of the water viscosity under nanoconfinements. In view of the similarity between nanochannels formed by the CNTs and those by the GE nanosheets, the water flow enhancement would also be expected for the GE bilayers. For a nonslip Poiseuille flow confined between two flat plate separated by a distance *d*, the flux rate by the HP equation Q_{HP} can be estimated as[20]

$$Q_{\mathrm{HP}} = \frac{d^2 \Delta P \rho N_{\mathrm{A}}}{12 \eta L} \quad , \tag{5}$$

where ρ and η are the molar density and viscosity of the bulk water, respectively, and N_{A} is the Avogadro constant. Define the enhancement factor as $\varepsilon = Q / Q_{\mathrm{HP}}$. By taking $\eta = 10^{-3}$ Pa s and $\rho = 0.0555$ mol/cm ^{3} , ε is calculated as 15.34 at $\Delta P = 5$MPa , indicating that the water flow rate in the GE bilayer is much larger than that predicted by classical continuum mechanics.

In the above calculations of Q and Q_{HP} , the channel thickness is taken as the interlayer distance of the GE layers. The simulation results show that vacuum space (~6 Å) forms between the water molecules and the GE layers due the water/GE vdW interactions. If this vacuum space

is subtracted from the channel thickness *d*, the water flow rate enhancement factor ε becomes even larger as ~240. A similar large enhancement factor has also been reported for water transport between layered GE nanosheets[20] and inside CNTs.[31] Previous studies have demonstrated that one reason for the significant water transport enhancement in nanochannels is the weak interaction between the water molecules and the confinement walls which results in a smooth surface with minimal even zero friction and thus leads to the molecule slippage along the walls.

One characteristic that could be used to understand the fast water transport inside the GE bilayers is the potential energy surface (PES) which describes the interaction energy between the water molecules and the GE layers at different locations. The PES has recently been proven to be critical for the understanding of the dynamics and transport behaviors at the atomic scales.[32-35] To calculate the PES, a water molecule is used as a probe to laterally scan the space between the GE layers. The potential energy is recorded as the water molecule probe moves. Fig. 3(a) shows part of the PES for the *XY* plane with a distance of 3.19 Å (a distance equal to the equilibrium vdW distance σ_{C-O} between the water molecules and the GE layer) away from the upper GE layer for the interlayer distance $d = 10$ Å. The minimal potential energy is set as zero for easy comparison.

It is noted that the minimum potential energy is around the hollow site of the honeycomb lattice structure while the maximum energy is around the site on top of the C atoms, which agrees well with previous work.[34] The energy corrugation among the minimum and maximum energy site is around 0.08 kcal/mol, which is much smaller than that of 0.5 kcal/mol found for water molecules inside the CNTs.[32] This small energy corrugation indicates the low friction between the GE layer and the water molecules and thus favors their movement from one site to

another without losing much of their mobility. The smaller energy corrugation of the GE bilayer than that of CNT also explains the higher water flow rate in the GE bilayer as discussed above.

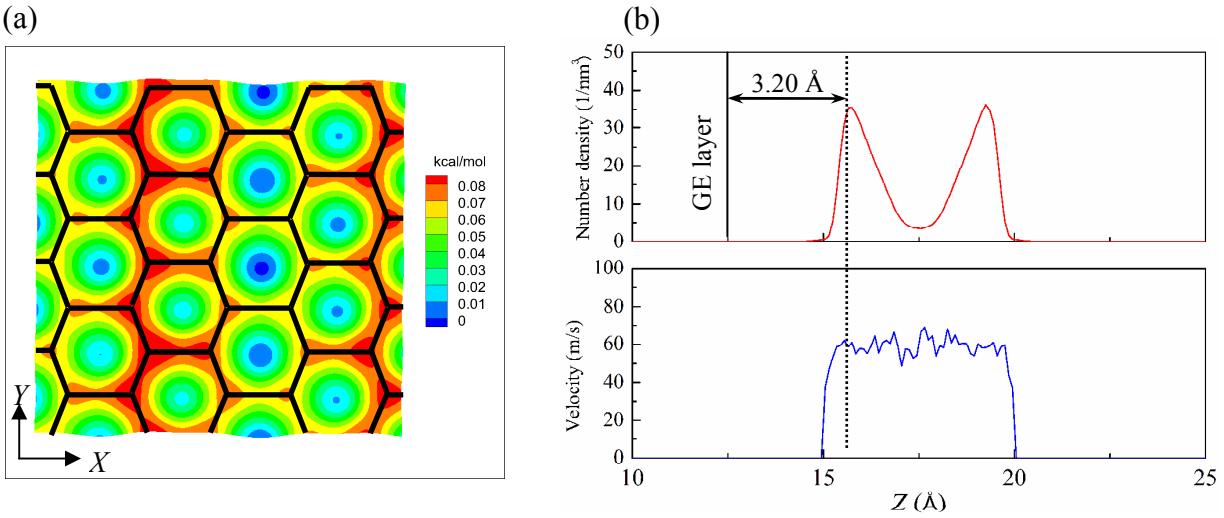

Fig. 3. (a) PES at the distance of 3.19 Å from the upper GE layer; (b) number density (up) and velocity (down) distribution along the water flow direction for the case of $d = 10$ Å and $\Delta P = 300$ MPa .

Fig. 3(b) shows the number density and velocity profiles of the water molecule across the channel thickness direction. Both the density and velocity profiles are calculated based on the O atoms. It is noted that two peaks appear in the density profile, implying that water molecules inside the GE bilayer tend to form layered structure. The distance between one water layer and its closest GE layer is around 3.20 Å which equals the equilibrium vdW distance of σ_{C-O}. At this distance, sharp jump is observed in the velocity profile, demonstrating that no boundary water layer is attached to the GE layer and thus a plug-like flow forms inside the channel. Such plug-like flow is the natural outcome of the low friction between the water molecules and the GE layers.

3.2. Channel thickness effect

To use layered GE or GO for nanofiltration and separation applications, a proper interlayer distance is usually desired. As the interlayer distance changes, the structure and dynamics of water molecules inside the layered GE structures alter. The dependence of the water flow rate Q on the channel thickness d is shown in Fig. 4(a). It is found that as d increases, Q increases monotonically.

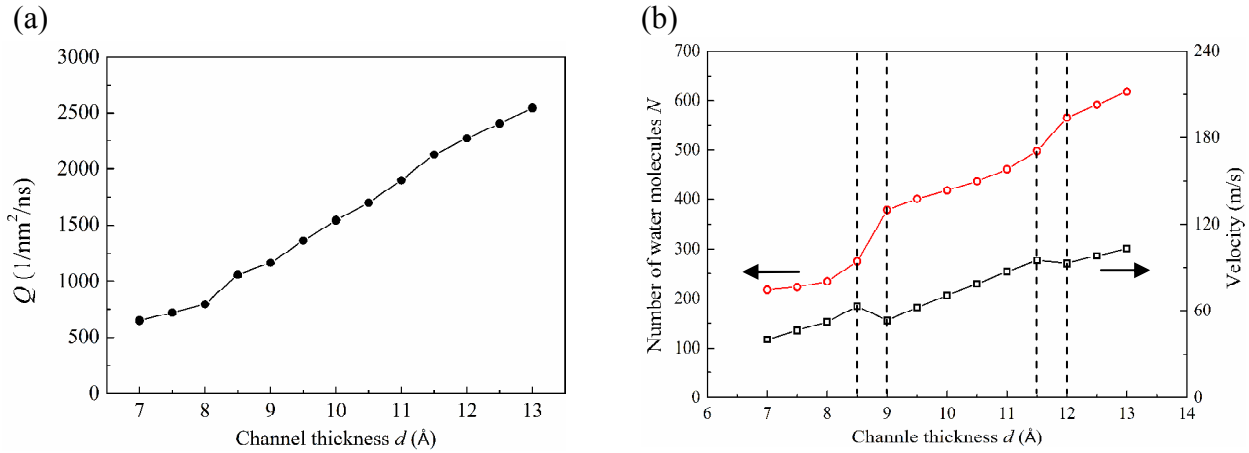

Fig. 4. (a) Dependence of the water flow Q on the channel thickness d; (b) dependence of the number N and average velocity $\bar{v}$ of water molecules in the channel on d.

For a given channel geometry, the water flow rate Q only depends on the average flow velocity $\bar{v}$ and the number N of the water molecules inside the channel, as indicated by Eq. (4). To understand the dependence of Q on the channel thickness d, both $\bar{v}$ and N are investigated for different d as plotted in Fig. 4(b). As d increases, both $\bar{v}$ and N show an overall increasing trend with a stepwise manner. For N, two sharp increases are observed in the regions of $8.5 < d < 9$ Å and $11.5 < d < 12$ Å, respectively. In these two regions, $\bar{v}$ reduces slightly.

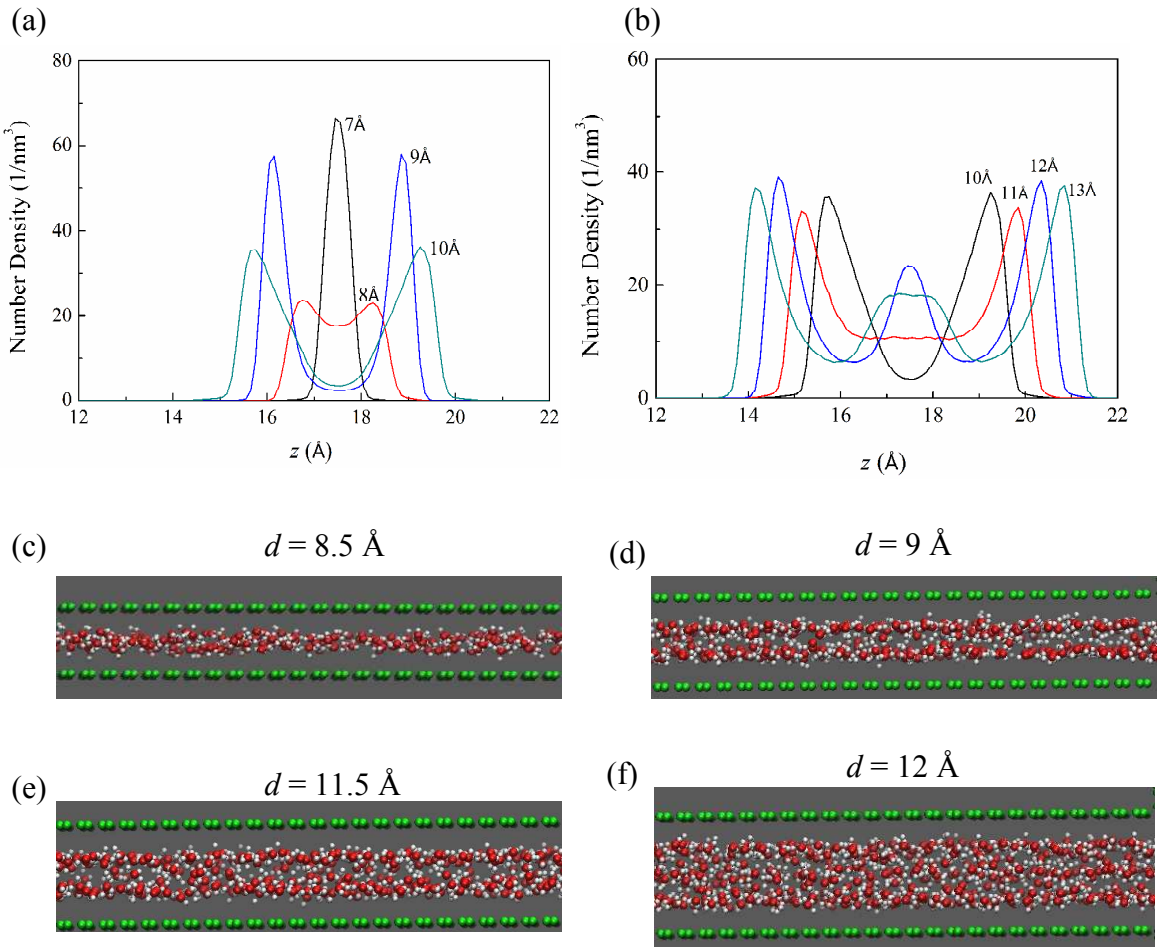

Fig. 5. (a) and (b) Density profile revolution as the channel thickness d increases from 7 to 13 Å; (c)-(f) water molecules arrangements for $d = 8.5, 9, 11.5, 12$ Å , respectively.

The stepwise increase in the number of the water molecule can be understood by exploring the water distributions in the GE bilayer. Figs. 5(a) and 5(b) show the evolution of the density profile along the channel thickness direction for the channel thickness d changing from 7 Å to 13 Å. As d increases from 7 to 10 Å, the density peak in the middle of the channel gradually splits into two new peaks which are close to the channel boundaries, i.e., the GE layers. As d further increases from 10 Å to 13 Å, a third peak appears in the middle of the channel. It should be noted that the most prominent change of the density profiles occurs when $8.5 < d < 9$ Å and

$11.5 < d < 12$ Å. For example, as d increases from 8.5 to 9 Å, the heights of the two peaks near the channel boundaries increase by almost 3 times.

By checking the distribution of the water molecules inside the nanochannel, it is found that the dramatic change of the water density profile is closely related to the formation of new water layers in the channel. As shown in Figs. 5(c) and 5(d), when d increases from 8.5 to 9 Å, the number of water layers increases from 1 to 2. Similar phenomenon can be observed when d increases from 11.5 to 12 Å, as shown in Figs. 5(e) and 5(f) where the water layer number further increases to 3. The increase of the water layers well explains the dramatic increase in the number of water molecules in the channel.

One difference between the water molecules distributions for $d = 9$ and $d = 12$ Å is that, the two water layers for the former case can be well recognized with few water molecules reside between the layers. However, for $d = 12$ Å there are more water molecules reside between the layers, and their interfaces become blurring which indicates that the water molecules distribution approaches to that of the bulk water. This water distribution transition can be further evidenced by the radial distribution function (RDF) for the O-O atom pairs inside the nanochannel as shown in Fig. 6. The RDF for bulk water is also plotted for comparison. For the bulk water, the first peak of the RDF, i.e., the first water shell, occurs at $r = 2.81$ Å, which agrees well with previous results.[36] For the water molecules confined between the GE bilayer with $d = 7$ Å, a second peak appears at $r = 5.56$ Å, indicating that the water molecules inside the channel are highly ordered in a long-range. As d increases, the peak magnitudes decrease and the RDFs get close to that for the bulk water. At $d = 13$ Å, the second peak that exists for $d = 7$ Å even disappears, which means that the long-range ordered water structure collapses gradually.

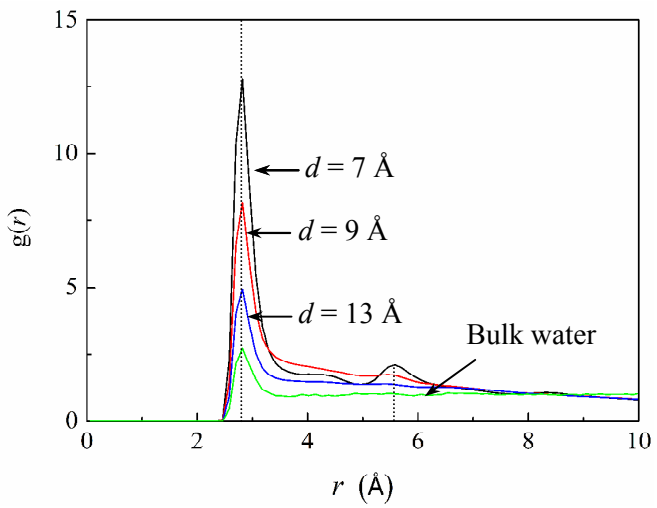

Fig. 6. RDFs for the O-O atom pairs inside the GE bilayer for different channel thickness *d*.

Previous studies have demonstrated that water diffusion inside nanochannels like CNTs is realized by hopping of water molecules from one site to another [37, 38]. With a reduced order of the water molecules, the water molecules would experience less constraints during hoping and thus a larger hoping rate can be expected which would favor their transport inside the channel. According to the previous studies, the hoping rate is linearly proportional to the diffusion coefficient *D* of the water molecules which can be simply estimated by their mean square displacement $\left\langle \Delta x^2(t) \right\rangle$ along the water flow direction through the relation $\left\langle \Delta x^2(t) \right\rangle \approx 2Dt$.[37, 38] Here, *t* denotes the simulation time. Fig. 7(a) shows the dependence of the diffusion coefficient *D* on the channel thickness *d*. During the calculation of $\left\langle \Delta x^2(t) \right\rangle$ for the estimation of *D*, the center of mass velocity is subtracted. It is observed that *D* increases monotonically as *d* increases, which indicates water molecules move more easily at larger *d*.

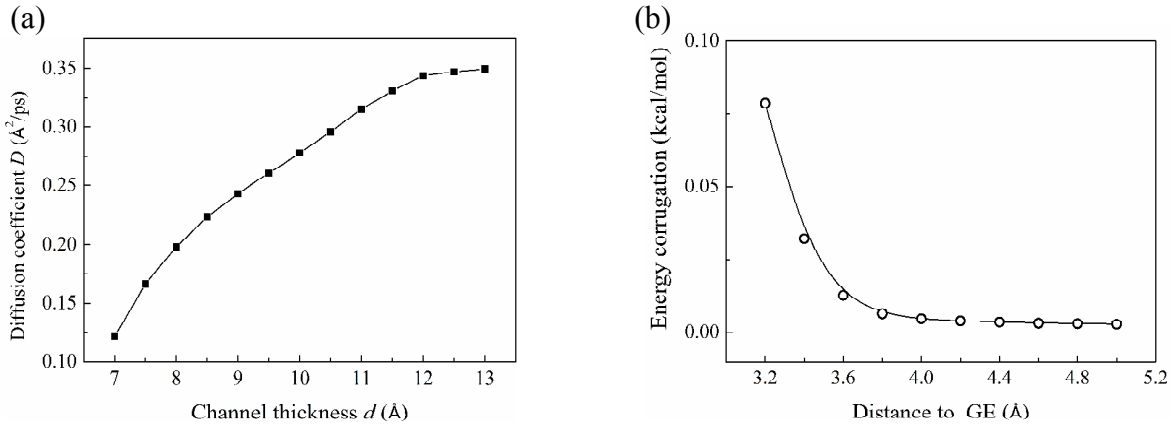

Fig. 7. (a) Dependences of the diffusion coefficient on the channel thickness *d* and (b) energy corrugation of the PES on its distance from the GE layer.

It should be noted that the reduced order of the water molecules arrangement is just one factor that contributes to the increase in their mobility. The decrease of the interaction strength between the water molecules and the GE layers with the increase of the interlayer distance *d* plays a more dominant role. Fig. 7(b) presents the dependence of energy corrugation of the PES on its distance from the GE layer. As the distance to the GE layer increases from the vdW equilibrium distance of $\sigma_{C-O} = 3.19$ Å, the PES energy corrugation decreases exponentially. When the distance of the PES to the GE layer increases from 3.20 to 3.60 Å, the energy corrugation decreases by almost 80%. The reduction of the energy corrugation implies that the interaction between the water molecule and the GE layer would be dramatically weakened as their distance increases and the energy barrier for the water movement would also significantly reduce. Hence, as the channel thickness *d* increases, the average distance between the water molecules and the GE layers would also increase, leading to weaker water-GE interaction and thus higher water molecule mobility.

To understand the effect of channel thickness on the average water molecule velocity shown in Fig. 4(b), the shearing stress τ between the water molecules and the GE layers is investigated. To calculate τ , the force f initially applied to drive the water flow is removed after the steady state is achieved. Afterwards, the simulation is conducted for 30 ps and during every 0.1 ps, the average velocity $\bar{v}$ of selected water molecules inside the channel is recorded. The molecules are selected based on their positions at the beginning of the simulation that their distance from the inlet of the channel is within the range of 10 to 20 Å. In this distance range, the effect of the inlet on the water transport becomes negligible. The simulation time of 30 ps is determined such that at the end of the simulation, all the selected molecules still reside inside the channel. The simulation shows that without the driving force, $\bar{v}$ decreases linearly with the time. From the deceleration a of the water molecules, the effective shearing stress between the GE bilayer and all the water molecules inside it is calculated as $\tau = Nma/(2LL_y)$. This method has also previously been used to calculate the shearing stress between the CNT and the water molecules within. [8]

Figs. 8(a) and 8(b) show the deceleration a and the effective shearing stress τ at different channel thicknesses d , respectively. As d increases, a decreases exponentially. This exponential decrease well reflects the exponential decay of the interaction strength between the water molecule and the GE layer as their distance increases (Fig. 7(b)). The shearing stress τ also shows an overall decreasing trend as d increases. Since τ is a function of both the deceleration a and the number of water molecules N inside the channel, two peaks are observed for τ at $d = 9$ and $d = 12$ Å, respectively, due to the sharp increase of N around this two point as shown in Fig. 4(b). A decreasing shearing stress means increasingly smooth surfaces of the GE layers for water

transport. Therefore, the average velocity $\bar{v}$ increases with d (Fig. 4(b)) and shows reduction at points $d = 9$ and $d = 12$ Å.

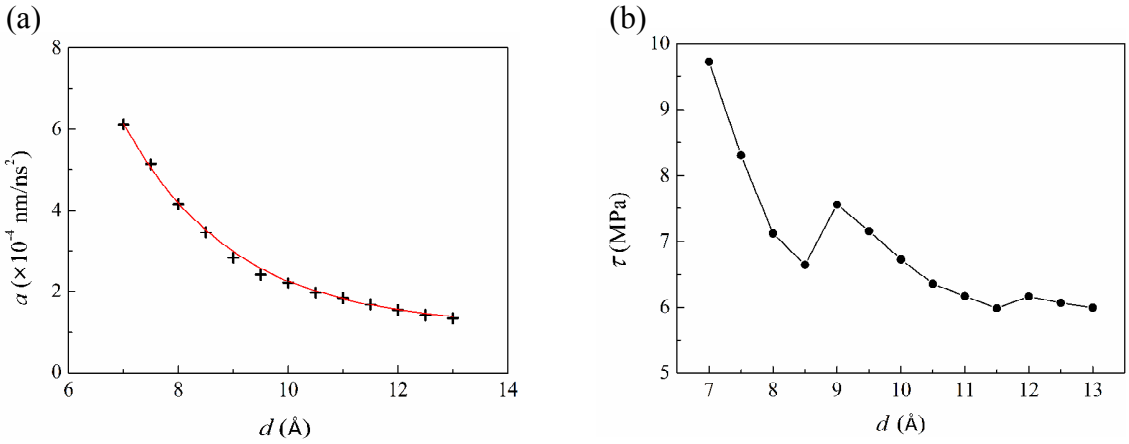

Fig. 8. (a) Deceleration a of the water molecules after the driving force f is removed and (b) the effective shearing stress τ for different channel thickness d.

3.3. Interaction strength effect

In the above simulations, pristine GE is modeled. However, in practical applications, GE is seldom produced at its pristine state. For the fabrication of GE using the chemical vapor deposition method, defects like void, impurity atoms and grain boundaries are usually inevitable. When GE is produced through reduction of the GO, complete reduction is also usually not achieved, which would lead to residual oxidation group on top of GE. When deviates from its pristine state, GE would interact with the water molecules with different interaction strengths and thus result in significantly different water transport behaviors. [20, 39]

In this study, the interaction strength between the water molecule and the GE layer is altered by changing the interaction scaling factor χ in Eq. (2) from 1 to 4. Fig. 9(a) shows the dependence of the water flow rate Q through the GE bilayer on the interaction strength scaling

factor χ for the case of $d = 10$ Å. It is demonstrated that Q decreases monotonically with the increase of χ.

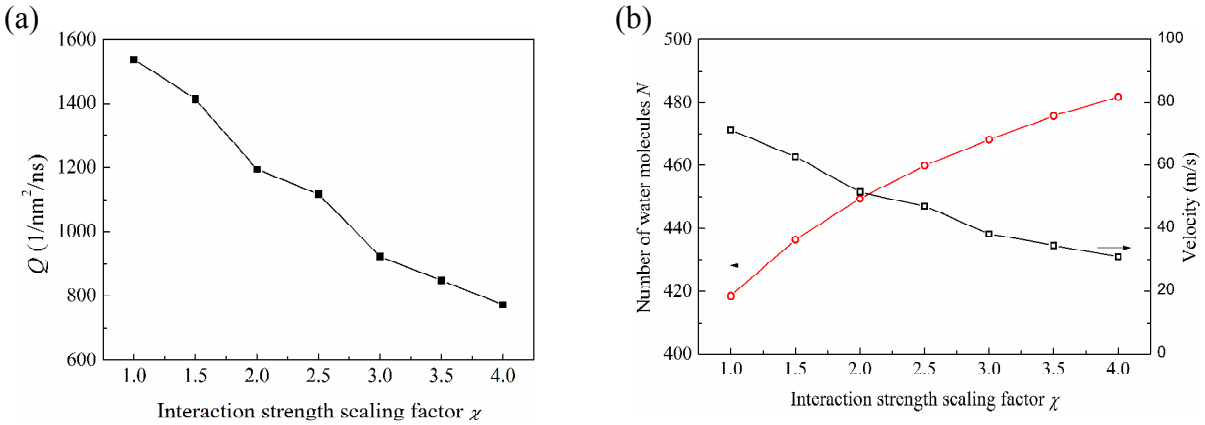

Fig. 9. Dependence of (a) the water flow Q, and (b) the number N and average velocity $\bar{v}$ of water molecules in the channel on interaction strength scaling factor χ.

Fig. 9(b) presents the number N of water molecules inside that channel and their average velocity $\bar{v}$ for different interaction strength χ. As χ increases, N increases while $\bar{v}$ decreases. However, the decreasing speed of $\bar{v}$ is much larger than the increasing speed of N. When χ increases from 1 to 4, $\bar{v}$ decreases by more than 50% while N increases no more than 15%. For a given channel geometry, $\bar{v}$ and N are the only factors that determine Q, thus it decreases as χ increases.

To further understand the effect of the interaction strength scaling factor χ on the water flow rate, the arrangement of the water molecules and their mobility are investigated. Figs. 10(a) and 10(b) show the RDFs for the O-O atom pairs and the density distribution profile along the channel thickness direction, respectively. It is found that as χ increases, the height of the second peak located at $r \approx 5.45$ Å of the RDF increases. Moreover, a third peak appears at $r \approx 8.25$ Å when χ increases to 4, as shown in the inset of Fig. 10(a). The change of the RDF with the

increase of χ indicates that the water molecules arrangement transforms from short-range ordered to long-range orders gradually as the interaction strength between the water and the GE layer increases.

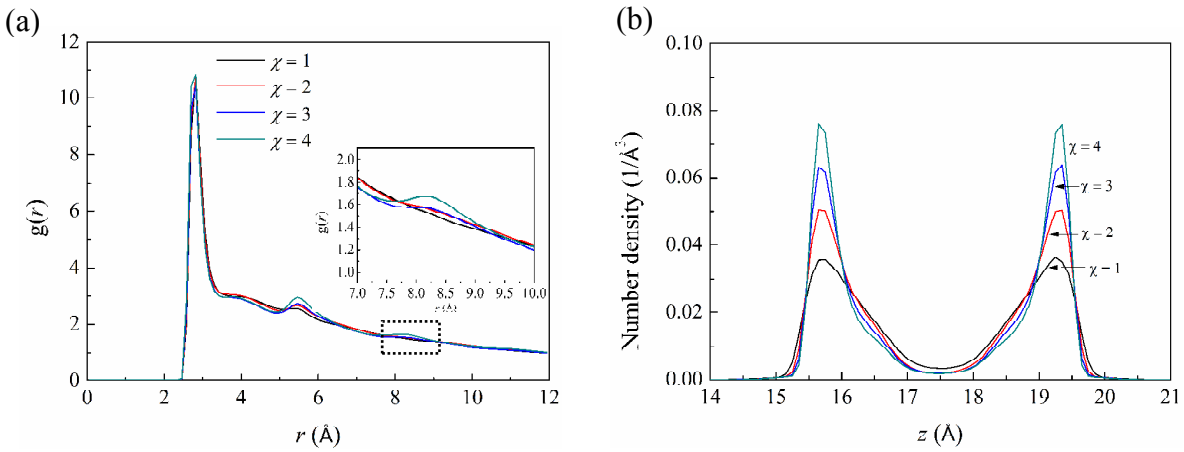

Fig. 10. (a) RDFs of the O-O atom pairs and (b) the density distribution profile along the channel thickness direction for different interaction strength scaling factor χ.

For the density distribution profile, the two peaks that are close to the two GE layers sharpen as χ increases. Furthermore, the heights of the peaks increase apparently, indicating that the water molecules prefer to reside near the GE layer at stronger interaction strengths. With a closer distance to the GE layers, the energy barriers for the water molecules to transport through the GE bilayer would be larger as demonstrated by Fig. 7(b). Thus, a smaller water flow rate occurs as the outcome.

The RDFs and the density distribution profile reflect the change of the water molecules arrangement inside the GE bilayer. Besides this change, the increase of the energy barrier for the water molecules transport with the increase of the interaction strength scaling factor χ plays a more dominant role in determining the water flow rate Q. The simulation results show that the

energy corrugation of the PES at the distance of 3.20 Å from the GE layer increases linearly with χ . Thus, the water flow rate decreases monotonically with χ .

3.4. Channel length effect

For a nonslip Poiseuille flow, the flow rate depends on the channel length as indicated by Eq. 5. This length-dependence of the flow rate mainly arises from the pressure loss along the flow direction due to the friction between the flow body and the confining walls. When water molecules flow inside nanochannels such as CNTs and the GE bilayers, the friction between the water molecules and the confining walls is so small that the pressure loss across the channel length becomes negligible.

Previous MD simulations have demonstrated that the water transport through the (10,0) CNT with a diameter of ~0.8 nm under the pressure of 100 MPa shows a water flow rate that is independent on the CNT length in the range of 2 to 10 nm.[40] Similar results have also been reported for the water transport in the (6,6) CNTs [41] and (7,7) CNTs [42] at driving pressures larger than 200 MPa. Interestingly, a recent MD study reported that when the driving pressure drops to 5 MPa, the resulting water flow in the CNTs shows significant dependence on their length.[29] One reasonable explanation for the different length-dependence of the water flow would be that the self-diffusion transport of the water molecules plays a more crucial role in the water flow rate for low driving pressure, but becomes ignorable when the pressure is high. According to the continuous-time random-walk modeled developed by Alexander *et al.*,[37] the diffusion of water molecules inside CNT is realized through their discrete hoping and shows exponential dependence on the CNT length. Hence, length-dependent water flow has been observed in CNTs with low driven pressure.

To investigate the length-dependence of the water transport inside the GE bilayer, the water flow rates Q for different bilayer length L are tested and shown in Fig. 11. The driving pressure difference is adopted as $\Delta P = 300$ MPa and the channel thickness d is set as 7 Å. It is found that the Q remains almost the same as L increases. However, when the vdW interactions between the water molecules and the GE layers are strengthened by 4 times, i.e., when the interaction strength scaling factor χ increases to 4; Q decreases dramatically as the L increases. These results demonstrate that for pressure-driven water flow confined in nanochannels, the weak interaction and thus the low friction between water and the channel walls are the key factors for achieving a fast flow rate. When the interaction is enhanced, the driving pressure decreases as the water body flows along the channel, leading to a slower and length-dependent flow rate.

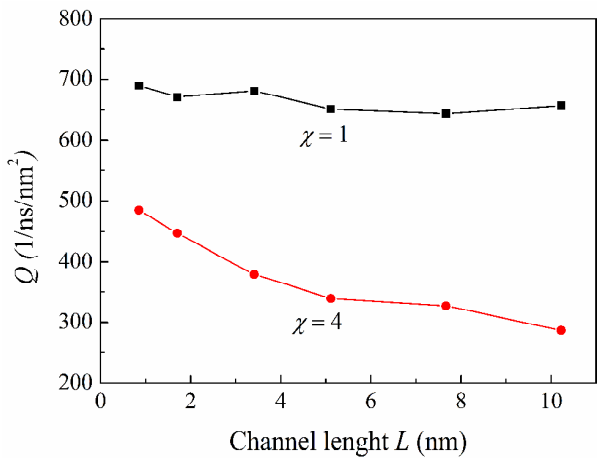

Fig. 11. Water flow rate Q inside the GE bilayer for different length L and interaction strength scaling factor χ .

4. Conclusions

MD simulations are conducted to investigate the water transport inside the nanochannel formed by the GE bilayers. The effects of the channel size, flow driving pressure as well as the

interaction strength between the water molecules and the GE bilayer are systematically studied. These effects are understood by exploring the spatial distribution of the water molecules, their flow velocity and the effective shearing stress.

It is found that ultrafast water flow rate Q can be observed inside the channel and increases linearly as the driving pressure increases. Linear extrapolation gives Q at the practical nanofiltration pressure of 5 MPa as 41.89 $(nm^2ns)^{-1}$, which is more than 15 times larger than that predicted by the classical HP equation. If consider the vacuum space formed between the water molecules and the GE layers, this enhancement factor can be even higher (~240). Such flow rate enhancement is attributed to the almost frictionless surface of the GE bilayer and the plug-like water flow formed inside it.

As the channel width d increases, the water flow rate Q increases monotonically. Such increase is mainly caused by the reduced friction force between the water flow and the GE layers due to their weakened interaction at an increasing average distance. On the contrary, the number of water molecules N inside the channel and their average velocity $\bar{v}$ which are the determining factors of Q , show nonmonotonic increase with d. Such nonmonotonic increases are attributed to the change of the spatial distribution of the water molecules as d increases. At small channel width d, the water molecules form ordered layer structure inside the channel. As d increases, more water molecules occupy the channel. At $d = 8.5$ and $d = 11.5$ Å, new water layers form inside the channel, leading two sharp increases of the water molecules. Such sharp increases enhance the total friction force between the water molecules and the GE layer, and thus lead to decreases of their average velocity $\bar{v}$ at $d = 8.5$ and $d = 11.5$ Å. As a result, $\bar{v}$ shows a nonmonotonic dependence on d.

In opposite to the effect of channel width, the water flow rate Q decreases as the interaction strength between the water molecules and the GE bilayer increases. Moreover, as the interaction strength increases, the water flow rate transforms from being independent on the channel length to monotonically decreasing with it. At larger interaction strengths, more water molecules occupy the channel but have lower average velocities. Moreover, the average velocity is more sensitive to the change of the interaction strength, thus leading to a decreasing water flow rate with the interaction strength. Meanwhile, at larger interaction strength, more water molecules tend to get close to the GE layers with enhanced order, which also reduces the average velocity.

Overall, the results from the present study provide useful information on the water transport inside GE bilayers. Recently, GO membranes show great potential in applications of nanofiltration and water purification. One key issue for the realization of these applications is the understanding of water transport between the nanochannels formed by the GO layers. The most significant difference between the water transport inside the GE layers and that inside the GO layers is the interaction strength, which has been considered in this study. Therefore, this study is of significant value for the design and application of GE-based nanomaterials in future nanofiltration and water purification technologies.

Acknowledgements

The authors acknowledge financial support from Ministry of Education, Singapore (Academic Research Fund TIER 1 - RG128/14) and the Nanyang Environment and Water Research Institute (Core Fund), Nanyang Technological University, Singapore.

References

1 N. Hilal, H. Al-Zoubi, N. A. Darwish, A. W. Mohammad and M. A. Arabi, *Desalination*, 2004,**170**:281-308.

2 H. Y. Yang, Z. J. Han, S. F. Yu, K. L. Pey, K. Ostrikov and R. Karnik. *Nat. commun.,* 2013,**4**: 10.

3 S. Prakash, M. Pinti and B. Bhushan, *Philos. Trans. R. Soc. A-Math. Phys. Eng. Sci.*, 2012,**370**:2269-303.

4 P. S. Waggoner and H. G. Craighead, *Lab Chip*, 2007,**7**:1238-55.

5 T. Kraus, L. Malaquin, H. Schmid, W. Riess, N. D. Spencer and H. Wolf, *Nat. Nanotechnol.*, 2007,**2**:570-6.

6 K. Salaita, Y. Wang and C. A. Mirkin, *Nat. Nanotechnol.*, 2007,**2**:145-55.

7 L. Liu, L. Zhang, Z. Sun and G. Xi, *Nanoscale*, 2012,**4**:6279-83.

8 X. Chen, G. Cao, A. Han, V. K. Punyamurtula, L. Liu, P. J. Culligan, *et al.*, *Nano Lett*. 2008,**8**:2988-92.

9 J. K. Holt, H. G. Park, Y. M. Wang, M. Stadermann, A. B. Artyukhin, C. P. Grigoropoulos, *et al.*, *Science*. 2006,**312**:1034-7.

10 M. Majumder, N. Chopra, R. Andrews and B. J. Hinds, *Nature*, 2005,**438**:44-.

11 G. Hummer, J. C. Rasaiah and J. P. Noworyta, *Nature*, 2001,**414**:188-90.

12 A. Striolo, *Nano Lett*., 2006,**6**:633-9.

13 K. Falk, F. Sedlmeier, L. Joly, R. R. Netz and L. Bocquet, *Nano Lett*., 2010,**10**:4067-73.

14 R. K. Joshi, P. Carbone, F. C. Wang, V. G. Kravets, Y. Su, I. V. Grigorieva, *et al.*, *Science*, 2014,**343**:752-4.

15 R. R. Nair, H. A. Wu, P. N. Jayaram, I. V. Grigorieva and A. K. Geim, *Science*, 2012,**335**:442-4.

16 B. Mi, *Science*. 2014,**343**:740-2.

17 H. W. Kim, H. W. Yoon, S.-M. Yoon, B. M. Yoo, B. K. Ahn, Y. H. Cho, *et al.*, *Science*, 2013,**342**:91-5.

18 H. Li, Z. Song, X. Zhang, Y. Huang, S. Li, Y. Mao, *et al.*, *Science*, 2013,**342**:95-8.

19 Y. Han, Y. Jiang and C. Gao, *ACS Appl. Mater. Interfaces*, 2015, **7**: 8147-8155.

20 N. Wei, X. Peng and Z. Xu, *ACS Appl. Mater. Interfaces,* 2014,**6**:5877-83.

21 S. Plimpton, *J. Comput. Phys.*,1995,**117**:1-19.

22 D. J. Price and C. L. Brooks, *J. Chem. Phys.*, 2004,**121**:10096-103.

23 A. D. MacKerell, D. Bashford, M. Bellott, R. L. Dunbrack, J. D. Evanseck, M. J. Field, *et al.*, *J. Phys. Chem. B*., 1998,**102**:3586-616.

24 T. Werder, J. H. Walther, R. L. Jaffe, T. Halicioglu and P. Koumoutsakos, *J. Phys. Chem. B*., 2003,**107**:1345-52.

25 F. Q. Zhu, E. Tajkhorshid and K. Schulten, *Biophys. J.*, 2002,**83**:154-60.

26 J. Su and H. Guo, *J. Phys. Chem. B*., 2012,**116**:5925-32.

27 T. A. Hilder, D. Gordon and S.-H. Chung, *Small*, 2009,**5**:2183-90.

28 H. Lu, J. Li, X. Gong, R. Wan, L. Zeng and H. Fang, *Phys. Rev. B*, 2008,**77**,174115.

29 L. Wang, R. S. Dumont and J. M. Dickson, *J. Chem. Phys.*, 2012,**137**,044102.

30 J. Goldsmith and C. C. Martens, *J. Phys. Chem. Lett.*, 2010,**1**:528-35.

31 J. A. Thomas and A. J. H. McGaughey, *Phys. Rev. Lett.*, 2009,**102**,184502.

32 Y.-C. Liu, J.-W. Shen, K. E. Gubbins, J. D. Moore, T. Wu and Q. Wang, *Phys. Rev. B*, 2008,**77**, 125438.

33 Y. Qiao, X. Xu and H. Li, *Appl. Phys. Lett.*, 2013,**103**, 233106.

34 G. Tocci, L. Joly and A. Michaelides, *Nano Lett.*, 2014,**14**:6872-7.

35 T. Wu, H. J. Werner and U. Manthe, *Science*, 2004,**306**:2227-9.

36 A. K. Soper, F. Bruni and M. A. Ricci, *J. Chem. Phys.*, 1997,**106**:247-54.

37 A. Berezhkovskii and G. Hummer, *Phys. Rev. Lett.*, 2002,**89**,064503.

38 J.-Y. Li, Z.-X. Yang, H.-P. Fang, R.-H. Zhou and X.-W. Tang, *Chin. Phys. Lett.*, 2007,**24**:2710-3.

39 M. Melillo, F. Zhu, M. A. Snyder and J. Mittal, *J. Phys. Chem. Lett.*, 2011,**2**:2978-83.

40 M. E. Suk and N. R. Aluru. *J. Phys. Chem. Lett.*, 2010,**1**:1590-4.

41 B. Corry. *J. Phys. Chem. B*., 2008,**112**:1427-34.

42 W. D. Nicholls, M. K. Borg, D. A. Lockerby and J. M. Reese, *Microfluid. Nanofluid.*, 2012,**12**:257-64.

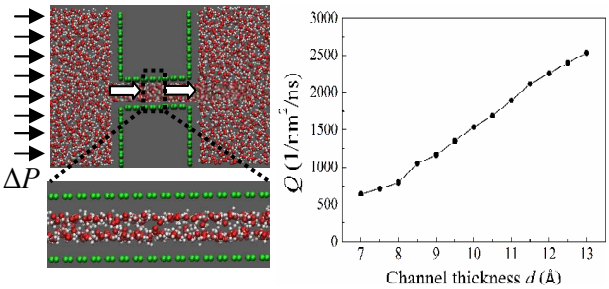

Water molecules form layered structure inside the graphene bilayers and ultra-high pressure-driven flow rate can be observed.